

AKADÉMIAI KIADÓ

Pollack Periodica •
An International Journal
for Engineering and
Information Sciences

16 (2021) 2, 98–103

DOI:
[10.1556/606.2020.00234](https://doi.org/10.1556/606.2020.00234)
© 2020 Akadémiai Kiadó, Budapest


ORIGINAL RESEARCH
PAPER



*Corresponding author.
E-mail: ulinuha14@mhs.ee.its.ac.id



Facial bones segmentation from skull point clouds based on deviation angle

Masy Ari Ulinuha^{1,2*} , Eko Mulyanto Yuniarno^{1,3},
I. Ketut Eddy Purnama^{1,3} and Mochamad Hariadi^{1,3}

¹ Department of Electrical Engineering, Faculty of Intelligent Electrical and Informatics Technology, Institut Teknologi Sepuluh Nopember, Surabaya, Indonesia

² Department of Information Technology, Faculty of Science and Technology, Universitas Islam Negeri Walisongo, Semarang, Indonesia

³ Department of Computer Engineering, Faculty of Intelligent Electrical and Informatics Technology, Institut Teknologi Sepuluh Nopember, Surabaya, Indonesia

Received: May 7, 2020 • Revised manuscript received: June 11, 2020 • Accepted: November 6, 2020
Published online: March 23, 2021

ABSTRACT

Facial bones segmentation is an important step to understanding a skull. In this paper, a method for segmenting facial bones from skull point clouds is proposed. The segmentation is based on the deviation angle features. The method consists of three phases: surface normal estimation, feature extraction, and point clouds classification. The method is applied to skull point clouds derived from computed tomography images. For evaluation, the method is compared with manual segmentation. The method has succeeded in segmenting facial bones with Precision = 0.836, Recall = 0.951, and $F = 0.890$.

KEYWORDS

facial bones, segmentation, skull point clouds, deviation angle

1. INTRODUCTION

Today, point clouds are a popular form of data for representing real-world 3D objects. Point clouds have been widely used to represent various objects, for example indoor scenes [1], outdoor scenes [2], buildings [3], trees [4], streets [5], and industrial sites [6]. Specific shapes can also be represented by point clouds, for example cars, motorbikes, tables, and chairs [7, 8]. Point clouds are also used to represent certain objects that are used for research purposes [9].

Point clouds store many information about the object they represent. To find out this information, a certain method is needed to better understand the point clouds. One technique that can be used in this case is segmentation [10]. Basically, point clouds segmentation techniques can be divided into Point Clouds Semantic Segmentation (PCSS) and Point Clouds Segmentation (PCS) [11]. PCSS tries to associate point clouds with semantic labels. Whereas PCS tries to group points based on certain geometric characteristics without associating with semantic labels.

A human skull is an object that can be represented by point clouds [12]. The skull is a center of study in various fields, including biometrics [13], craniofacial surgery [14], detection of abnormalities [15], and craniofacial reconstruction [16]. The skull has many information that can be explored. Point clouds segmentation can be an appropriate instrument for enriching the skull with semantic information.

The main region of a skull is the facial bones. The facial bones provide many information needed for various purposes. The facial bones consist of 14 different bones. This collection of bones forms the facial structure [17]. To separate the facial bones, segmentation techniques are needed.

Skull segmentation can also be done manually, but it will be time consuming and depends on human skills. Therefore the human intervention needs to be reduced and even eliminated from the segmentation process. Several methods of skull segmentation have been proposed. The existing segmentation methods can be grouped into three, registration-based, landmark-based and feature-based methods. The registration-based method begins with manual segmentation of the reference skull then a registration process is performed to segment the target skulls. The landmark-based method divides the skull into several regions by connecting several skull landmarks. The feature-based method seeks to acquire the skull region based on features extracted on the skull.

Deng et al. [18], Duan et al. [19], and Hu et al. [20] proposed registration-based segmentation. Deng divided the skull into seven regions. Six of them are the left eye, right eye, nose, mouth, left ear, and right ear. The skull region besides the six was called the frame. In other study, Duan divided the skull into five regions, the left eye, right eye, nose, mouth, and frame. In another study, Hu divided the skull into three regions, the eyes, nose, and mouth. In the three studies, segmentation of the reference skull was done manually while segmentation of the target skulls was obtained by correspondence. This registration-based segmentation requires manual segmentation of the reference skull. Manual segmentation made this method not fully automatic. On the other hand, the registration is not a simple process.

Landmark-based segmentation was proposed by Zhang et al. [21] and Tilotta et al. [22]. Landmarks are certain points on the skull where the thickness of soft tissue is measured [23]. Zhang divided the skull into five regions, the left eye, right eye, nose, mouth, and a region other than the four. The landmarks were selected semi-automatically. Then, a deformable template was created for each segment. This deformable template was based on the geometric characteristics of each segment. Next, the deformable template parameter was adjusted to the landmarks that have been selected. In Tilotta's study, the chin and the nose were segmented. The chin was determined by several landmarks, namely right mental, gnathion, left mental, and infradental points, while the nose was determined by right infraorbital, prosthion, infraorbital, and nasion points. In this method, it was necessary to determine the landmark positions. Determining landmarks manually was not easy, whereas automatic landmark detection was a complicated task.

To eliminate human intervention, Pei et al. [24] proposed feature-based segmentation method. He uses 2D depth maps as a basis for feature extraction. A point is said to be a feature if it has greater depth differences compared to its neighbors. Segmentation is done to get the left eye, right eye, nose, and mouth region. The regions of each segment are determined based on the Euclidean distance from the feature to a point. This method successfully divides regions in the skull automatically. In this method, the success of segmentation was determined by the success of feature extraction.

Up to the time of writing this paper, there are no studies that specifically discuss facial bones segmentation in skull

point clouds. Meanwhile many anatomical information can be obtained from the facial bones, including the position of the nose and mouth [23]. In this paper, a new method for facial bones segmentation in skull point clouds is proposed. The segmentation is based on the deviation angle. Based on the deviation angle features, each point is classified into two regions, namely facial bones and non-facial bones. The purpose of this study is to design an accurate facial bones segmentation method.

2. DEVIATION ANGLE

In this paper, the deviation angle is defined as the angle formed by a surface normal and a reference vector. The surface normal contains information that indicates the orientation of the surface [25].

The basic idea of the deviation angle is to create a reference vector at each point in skull point clouds. The direction of the reference is then compared with the surface normal. The angle formed by the reference and the normal is called the deviation angle. Assuming that the shape of the skull is close to a sphere, the reference is determined as a vector that passes through the centroid and a point on the surface of the skull. Figure 1 shows the surface of the skull along with normal and reference vectors.

To simplify the computation, the dot product of the normal and the reference is used to represent the deviation angle. To avoid distortion, the normal and the reference are expressed in unit vectors. The dot product is large when the deviation is close to 0° , and small when the deviation is close to 90° . If the unit vector of the normal is \hat{n} and the unit vector of the reference is \hat{a} , then the dot product v at a point on the the surface is

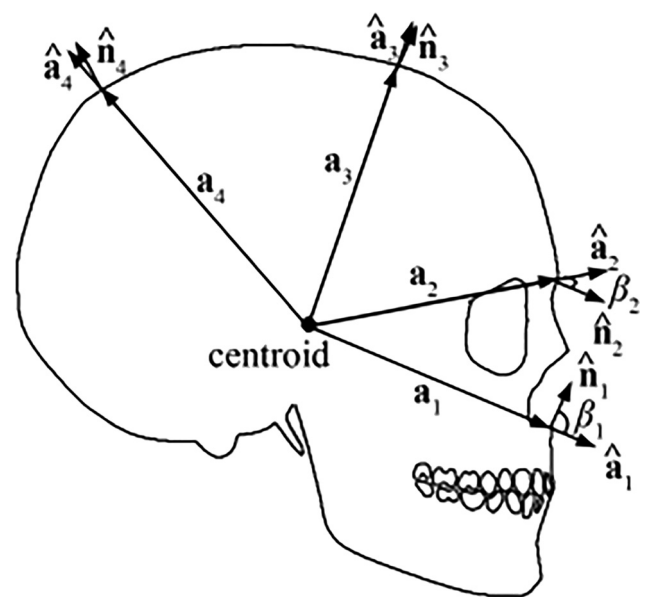


Fig. 1. A skull with reference vector (\mathbf{a}_i); unit reference vector ($\hat{\mathbf{a}}_i$); unit normal vector ($\hat{\mathbf{n}}_i$); and deviation angle (β_i)

$$v = \hat{n} \cdot \hat{a} = \|\hat{n}\| \|\hat{a}\| \cos \beta = \cos \beta, \quad (1)$$

where β is the deviation angle. From Eq. (1), it is expected to get more small values in the facial bones region, and more large values in the non-facial bones region.

3. MATERIALS AND METHODS

The data used in this study are skull point clouds from 23 patients in a hospital. Each point cloud derived from Computed Tomography (CT) images of the head of each patient, and each head consists of 316–519 CT image slices. The CT images are saved in the format of Digital Imaging and Communications in Medicine (DICOM). From the CT images, the skull bones are obtained by applying the thresholding technique. The threshold value is based on the Hounsfield Unit (HU) value of cortical bone [26]. Next, scanning technique is used to get the outermost contours of the skull [27]. These contours are then reconstructed into skull point clouds based on information obtained from the metadata of the DICOM file [28]. The neck of each skull is removed manually, as well as medical equipment that are accidentally included in the point clouds. Finally, there are 23 skull point clouds, which each point cloud consists of 198,528 to 293,126 points. All skulls are normal, except for one broken skull.

The skull point clouds as input, can be expressed as

$$\mathbf{P} = [\mathbf{p}_1, \mathbf{p}_2, \dots, \mathbf{p}_m]^T, \quad (2)$$

where m is the number of points and $\mathbf{p}_i = [p_{ix}, p_{iy}, p_{iz}]^T$ represents the position of a point in three-dimensional coordinates.

In this study, a method is developed for facial bones segmentation from the skull point clouds.

The method consists of three stages. First, the surface normal is estimated at each point. Second, the facial and non-facial bone features are extracted based on the deviation angle. Third, each point in the point clouds is classified based on the features. In the classification process, a rule is developed based on the number of features found around the point. The segmentation method is shown in Fig. 2.

3.1. Surface normal estimation

Surface normal of a point clouds can be estimated by various methods. In this study, plane PCA [25, 29] is used to

estimate the normal at each point on the skull surface. For each point $\mathbf{p}_i \in \mathbf{P}$, a normal vector $\mathbf{n}_i = [n_{ix}, n_{iy}, n_{iz}]^T$ is estimated. The normal vector is then converted into its unit vector $\hat{\mathbf{n}}_i = \mathbf{n}_i / \|\mathbf{n}_i\|$. The normal vectors of all points in \mathbf{P} are represented by

$$\mathbf{N} = [\hat{\mathbf{n}}_1, \hat{\mathbf{n}}_2, \hat{\mathbf{n}}_3, \dots, \hat{\mathbf{n}}_m]^T. \quad (3)$$

After normal vectors of all points are obtained, it is necessary to check the direction of the normal. The direction is compared with skull centroid $\bar{\mathbf{P}} = \left(\sum_{i=1}^m \mathbf{p}_i \right) / m$. The direction is correct if it is leaving the centroid, and wrong otherwise. For normal vectors that are misdirected, the direction will be inverted to satisfy

$$\|\mathbf{a}_i\| < \|\mathbf{a}_i + \hat{\mathbf{n}}_i\|. \quad (4)$$

3.2. Feature extraction

The shape of the skull is similar to a sphere. However, the surface of the face has a variety of shapes. With this variation, it is expected to obtain some features on the face. The deviation angle concept is used to extract the features. At each point $\mathbf{p}_i \in \mathbf{P}$, the dot product of the reference and the normal is calculated using equation

$$v_i = \hat{\mathbf{n}}_i \cdot \hat{\mathbf{a}}_i. \quad (5)$$

In a three-dimensional Euclidean space, Eq. (5) can be solved as follows

$$v_i = n_{ix}a_{ix} + n_{iy}a_{iy} + n_{iz}a_{iz}. \quad (6)$$

The results of the dot product at all points are then expressed as $\mathbf{V} = [v_1, v_2, v_3, \dots, v_m]$. The results are sorted in ascending order to $\mathbf{V}^{(s)} = [v_1, v_2, v_3, \dots, v_m]$, where $v_i \leq v_{(i+1)}$. From $\mathbf{V}^{(s)}$ the smallest and the largest values are recorded. The values \mathbf{V}_1 and \mathbf{V}_2 are expressed as

$$\mathbf{V}_1 = [v_1, v_2, v_3, \dots, v_j]^T | j = \text{round}(\alpha m), \quad (7)$$

$$\begin{aligned} \mathbf{V}_2 &= [v_{m-k}, v_{m-k+1}, v_{m-k+2}, \dots, v_m]^T | k \\ &= \text{round}(\alpha m) - 1, \end{aligned} \quad (8)$$

where $0 \leq \alpha \leq 1$ and $\text{round}(\alpha m)$ is rounding the value of αm .

The points corresponding to \mathbf{V}_1 and \mathbf{V}_2 are the features. These features are called: the deviation angle features. The features are expressed as

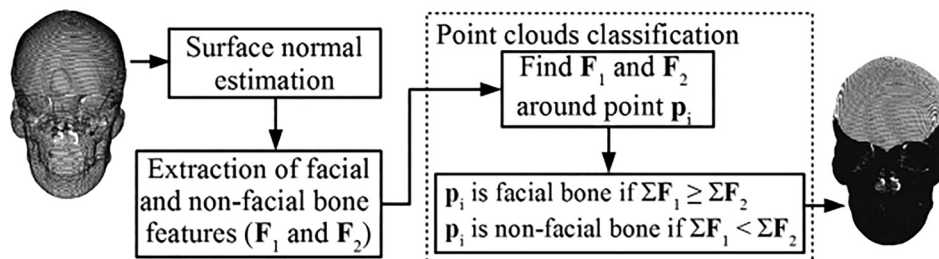


Fig. 2. Segmentation method

$$\mathbf{F}_1 = [\mathbf{b}_{11}, \mathbf{b}_{12}, \mathbf{b}_{13}, \dots, \mathbf{b}_{1j}]^T, \quad (9)$$

$$\mathbf{F}_2 = [\mathbf{b}_{21}, \mathbf{b}_{22}, \mathbf{b}_{23}, \dots, \mathbf{b}_{2k}]^T, \quad (10)$$

where $\mathbf{b}_{1i} \in \mathbf{P}$ and $\mathbf{b}_{2i} \in \mathbf{P}$ are the points corresponding to \mathbf{V}_1 and \mathbf{V}_2 . \mathbf{F}_1 is the feature for facial bones and \mathbf{F}_2 is the feature for non-facial bones.

3.3. Point clouds classification

The deviation angle features are used to classify the skull point clouds. Point \mathbf{p}_i will be classified as facial bone if there are more facial bone features around it than non-facial bone features, otherwise, \mathbf{p}_i will be classified as non-facial bone.

To find out the number of features around \mathbf{p}_i , it is sought all the deviation angle features that are neighbors of \mathbf{p}_i . All $\mathbf{b}_{1j} \in \mathbf{F}_1$ and $\mathbf{b}_{2k} \in \mathbf{F}_2$ with distance s from \mathbf{p}_i are recorded. Points \mathbf{b}_{1j} and \mathbf{b}_{2k} are included as the neighbors of \mathbf{p}_i if they meet equation

$$d(\mathbf{p}_i, \mathbf{b}) \leq s, \quad (11)$$

where $d(\mathbf{p}_i, \mathbf{b}) = \|\mathbf{p}_i - \mathbf{b}\|$ is the Euclidean distance from \mathbf{p}_i to \mathbf{b} . The neighboring features of \mathbf{p}_i are then expressed as

$$\mathbf{R} = [\mathbf{b}_{11}, \mathbf{b}_{12}, \mathbf{b}_{13}, \dots, \mathbf{b}_{1h}, \mathbf{b}_{21}, \mathbf{b}_{22}, \mathbf{b}_{23}, \dots, \mathbf{b}_{2l}]^T, \quad (12)$$

where \mathbf{R} is the matrix of the neighboring features, h is the number of facial bones features, and l is the number of non-facial bones features.

Then \mathbf{R} is used as the basis for classifying \mathbf{p}_i . Point \mathbf{p}_i is classified as facial bone if $h \geq l$, and as non-facial bone if $h < l$. The classification is implemented in equation.

$$c(\mathbf{p}_i) = \begin{cases} 0, & \text{if } h \geq l, \\ 1, & \text{if } h < l, \end{cases} \quad (13)$$

where $c(\mathbf{p}_i) = 0$ means \mathbf{p}_i is facial bone, and $c(\mathbf{p}_i) = 1$ means \mathbf{p}_i is non-facial bone.

4. RESULT AND DISCUSSION

The proposed method is implemented on 23 skull point clouds. The method has successfully segmented the facial bones. To evaluate the performance of the method, the results are compared with manual segmentation.

4.1. Manual segmentation

Manual segmentation is used as a comparison of the proposed method. Manual segmentation is performed on the skull point clouds in lateral view. To simplify the problem, the facial bones are defined as a region, which is bounded by three cranial landmarks, namely Frontotemporale (ft), Porion (po), and Gonion (go). The definitions of these landmarks are explained in [23]. Figure 3 shows the results of manual segmentation.

4.2. Segmentation results

The result of facial bones segmentation is declared successful if all facial bones are detected as facial bones, and all non-facial bones are detected as non-facial bones. Figure 4 shows the results of facial bones segmentation. The figure shows that most of the facial bones are successfully segmented.

The results of facial bones segmentation are compared with manual segmentation. It is assumed that the results of manual segmentation are the correct results.

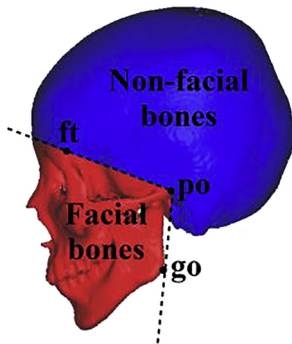


Fig. 3. The result of manual segmentation

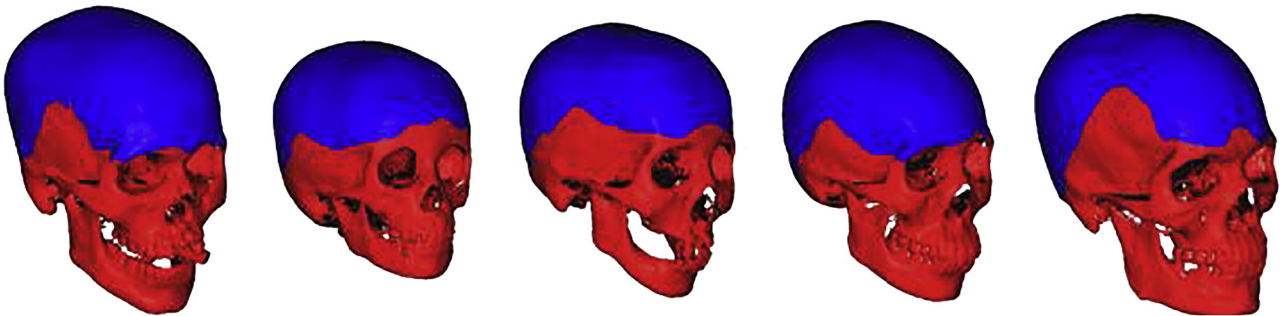


Fig. 4. The results of facial bones segmentation

When the segmentation results are compared with the correct results, there are four conditions. The four conditions as it is shown in Table 1 are: True Positive (TP), False Positive (FP), False Negative (FN) and True Negative (TN). As it is shown in Table 1, in the segmentation results, the facial bones area is declared as Segmented condition Positive (SP), and the non-facial bones area is declared as Segmented condition Negative (SN). As for the correct results, the region of facial bones is declared as Correct condition Positive (CP), and the region of non-facial bones is declared as Correct condition Negative (CN). For further explanation please refer to [30].

4.3. Precision, recall, and F measure

To measure the success rate of facial bone segmentation quantitatively, precision, recall and F measure are calculated. These measures have been widely used in the detection algorithm and can be applied to image segmentation [31]. These measures are calculated using equations

$$\text{Precision} = \frac{|TP|}{|SP|}, \quad (14)$$

$$\text{Recall} = \frac{|TP|}{|CP|}, \quad (15)$$

$$F = \frac{2 \cdot \text{Precision} \cdot \text{Recall}}{\text{Precision} + \text{Recall}}. \quad (16)$$

The segmentation experiments are performed by varying the value of α in Eq. (7) and Eq. (8). The value of α is varied between 0.01 and 0.1. The value of s in Eq. (11) is also made

to vary by giving it a value between 10 mm and 100 mm. The precision and recall in each experiment are calculated, and then the precision and recall values that maximize the F measure are recorded. α and s when F measure reaches the maximum value are also recorded. These values are shown in Table 2.

Table 2 shows that the average precision is 0.836. This value indicates that more than 83% of the points in the segmentation result are actually facial bones. Maximum precision is obtained by Skull_22, the value is 0.896. While the minimum precision is 0.736, this value is obtained by Skull_13. This happens because Skull_13 is a broken skull.

Recall calculations get an average of 0.951. This shows that more than 95% of the facial bones area in the manual segmentation is actually detected by the proposed method. Skull_17 gets the maximum recall value, which is 0.985, while the minimum recall value is obtained by Skull_15 with a value of 0.910.

The calculation results also show that the average value of the F measure is 0.890. This value indicates that the proposed method successfully segmented the facial bones. The success rate for the method is 89%. The maximum F measure is 0.935, which is achieved by Skull_17. This data also gets the best recall value. Skull_13 gets the minimum F measure, which is 0.836. This data also gets the minimum precision. Thus, based on the F measure, the best segmentation result is achieved by Skull_17 and the worst is Skull_13.

5. CONCLUSION

In this paper, a method for segmenting facial bones in skull point clouds has been proposed. The method is based on a feature called the deviation angle feature. The proposed method is successful in facial bones segmentation by achieving Precision = 0.836, Recall = 0.951, and F = 0.890.

Further research can be directed at increasing precision by reducing the area of false positives. This is very important especially for abnormal skulls. Abnormal skulls may require special treatment.

Table 1. Confusion matrix

		Manual Segmentation	
		CP	CN
Segmentation Result	SP	TP	FP
	SN	FN	TN

Table 2. Precision, recall, F measure, α , and s in centimeter

Point clouds	Precision	Recall	F measure	α	s	Point clouds	Precision	Recall	F measure	α	s
Skull_1	0.84	0.954	0.894	0.03	2	Skull_13	0.736	0.967	0.836	0.1	3
Skull_2	0.875	0.948	0.91	0.01	2	Skull_14	0.853	0.942	0.895	0.02	2
Skull_3	0.822	0.984	0.896	0.01	2	Skull_15	0.866	0.908	0.887	0.01	2
Skull_4	0.835	0.983	0.903	0.01	2	Skull_16	0.841	0.944	0.89	0.02	2
Skull_5	0.878	0.93	0.903	0.02	2	Skull_17	0.89	0.985	0.935	0.03	2
Skull_6	0.804	0.943	0.868	0.02	2	Skull_18	0.824	0.971	0.892	0.01	2
Skull_7	0.809	0.95	0.872	0.04	2	Skull_19	0.857	0.937	0.895	0.01	2
Skull_8	0.83	0.927	0.876	0.1	2	Skull_20	0.849	0.965	0.904	0.09	3
Skull_9	0.804	0.934	0.864	0.01	3	Skull_21	0.799	0.967	0.875	0.03	3
Skull_10	0.848	0.944	0.894	0.01	2	Skull_22	0.896	0.92	0.908	0.03	2
Skull_11	0.84	0.959	0.896	0.05	2	Skull_23	0.824	0.958	0.886	0.02	2
Skull_12	0.812	0.962	0.881	0.01	2	Average	0.836	0.951	0.89		

REFERENCES

- [1] R. Honti, J. Erdélyi, and A. Kopáčík, “Plane segmentation from point clouds,” *Pollack Period.*, vol. 13, no. 2, pp. 159–171, 2018.
- [2] L. Wang, Y. Huang, Y. Hou, S. Zhang, and J. Shan, “Graph attention convolution for point cloud semantic segmentation,” in *IEEE/CVF Conference on Computer Vision and Pattern Recognition*, Long Beach, CA, USA, June 15–20, 2019, 2019, pp. 10288–10297.
- [3] Y. Xu, W. Yao, S. Tuttas, L. Hoegner, and U. Stilla, “Unsupervised segmentation of point clouds from buildings using hierarchical clustering based on gestalt principles,” *IEEE J. Sel. Top. Appl. Earth Obs. Remote Sens.*, vol. 11, no. 11, pp. 4270–4286, 2018.
- [4] M. Shahzad, M. Schmitt, and X. X. Zhu, “Segmentation and crown parameter extraction of individual trees in an airborne tomosar point cloud,” *Int. Arch. Photogr. Remote Sens. Spat. Inf. Sci.*, vol. XL-3/W2, pp. 205–209, 2015.
- [5] C. Choy, J. Gwak, and S. Savarese, “4D spatio-temporal convnets: Minkowski convolutional neural networks,” in *IEEE/CVF Conference on Computer Vision and Pattern Recognition*, Long Beach, CA, USA, June 15–20, 2019, 2019, pp. 3070–3079.
- [6] T. Rabbani, F. van den Heuvel, “Efficient hough transform for automatic detection of cylinders in point clouds,” in *ISPRS Workshop on Laser Scanning*, vol. 3, Enschede, The Netherlands, Sep. 12–14, 2005, 2005, pp. 60–65.
- [7] X. Wang, S. Liu, X. Shen, C. Shen, and J. Jia, “Associatively segmenting instances and semantics in point clouds,” in *IEEE/CVF Conference on Computer Vision and Pattern Recognition*, Long Beach, CA, USA, June 15–20, 2019, 2019, pp. 4091–4100.
- [8] W. Wang, R. Yu, Q. Huang, and U. Neumann, “SGPN: Similarity group proposal network for 3D point cloud instance segmentation,” in *IEEE/CVF Conference on Computer Vision and Pattern Recognition*, Salt Lake City, UT, USA, June 18–23, 2018, 2018, pp. 2569–2578.
- [9] T. T. Tran, V. T. Cao, and D. Laurendeau, “Extraction of cylinders and estimation of their parameters from point clouds,” *Comput. Graphics*, vol. 46, pp. 345–357, 2015.
- [10] R. Honti, J. Erdélyi, and A. Kopáčík, “Automation of cylinder segmentation from point cloud data,” *Pollack Period.*, vol. 14, no. 3, pp. 189–200, 2019.
- [11] Y. Xie, J. Tian, and X. X. Zhu, “Linking points with labels in 3d: A review of point cloud semantic segmentation,” *IEEE Geosci. Remote Sens. Mag.*, 2020, doi: 10.1109/MGRS.2019.2937630.
- [12] Y. Wen, Z. Mingquan, G. Guohua, and L. Xiaoning, “A hierarchical skull point cloud registration method,” *IEEE Access*, vol. 7, pp. 132609–132618, 2019.
- [13] L. Benarous, B. Kadri, and A. Bouridane, “A survey on cyber security evolution and threats: Biometric authentication solutions,” in *Biometric Security and Privacy*, R. Jiang, S. Al-Maadeed, and A. Bouridane, eds, Springer, 2017, pp. 371–411.
- [14] M. Davey, N. M. McNerney, T. Barry, A. Hussey, and S. Potter, “Virtual surgical planning computer-aided design-guided osteo-cutaneous fibular free flap for craniofacial reconstruction: A novel surgical approach,” *Cureus*, vol. 11, no. 11, Paper no. e6256, 2019.
- [15] L. Imbruglia, A. Cacciatore, S. Carrara, S. Recupero, T. La Galia, E. M. Pappalardo, and A. Mammaro, “Abnormal skull findings in neural tube defects,” *J. Prenatal Med.*, vol. 3, no. 3, pp. 44–47, 2009.
- [16] W. J. Lee, V. Shinde, Y. J. Kim, E. J. Woo, N. Jadhav, P. Waghmare, Y. Yadav, A. Munshi, A. Panyam, M. Chatterjee, C. S. Oh, J. H. Hong, C. M. Wilkinson, V. Rynn, and D. H. Shin, “Craniofacial reconstruction of the Indus valley civilization individuals found at 4500-year-old Rakhigarhi cemetery,” *Anatomical Sci. Int.*, vol. 95, no. 2, pp. 286–292, 2020.
- [17] J. R. Jenkins, *Atlas of Neuroradiologic Embryology, Anatomy, and Variants*. Philadelphia: Lippincott Williams & Wilkins, 2000.
- [18] Q. Deng, M. Zhou, Z. Wu, W. Shui, and Y. Ji, “A regional method for craniofacial reconstruction based on coordinate adjustments and a new fusion strategy,” *Forensic Sci. Int.*, vol. 259, pp. 19–31, 2016.
- [19] F. Duan, D. Huang, Y. Tian, K. Lu, Z. Wu, and M. Zhou, “3D face reconstruction from skull by regression modeling in shape parameter spaces,” *Neurocomputing*, vol. 151, no. P2, pp. 674–682, 2015.
- [20] Y. Hu, F. Duan, B. Yin, M. Zhou, Y. Sun, Z. Wu, and G. Geng, “A hierarchical dense deformable model for 3D face reconstruction from skull,” *Multimed. Tools Appl.*, vol. 64, no. 2, pp. 345–364, 2013.
- [21] K. Zhang, Y. Cheng, and W. K. Leow, “Dense correspondence of skull models by automatic detection of anatomical landmarks,” in *Computer Analysis of Images and Patterns*. R. Wilson, E. Hancock, A. Bors, and W. Smith, eds, Springer, 2013, pp. 229–236.
- [22] F. M. Tilotta, J. A. Glaunes, F. J. P. Richard, and Y. Rozenholc, “A local technique based on vectorized surfaces for craniofacial reconstruction,” *Forensic Sci. Int.*, vol. 200, no. 1–3, pp. 50–59, 2010.
- [23] M. Y. Iscan and M. Steyn, *The Human Skeleton in Forensic Medicine*. Springfield, Illinois: Charles C Thomas, 2013.
- [24] Y. Pei, H. Zha, and Z. Yuan, “Creating a face model from an unknown skull based on the tissue map,” in *15th IEEE International Conference on Image Processing*, San Diego, CA, USA, Oct. 12–15, 2008, 2008, pp. 2088–2091.
- [25] K. Klasing, D. Althoff, D. Wollherr, and M. Buss, “Comparison of surface normal estimation methods for range sensing applications,” in *IEEE International Conference on Robotics and Automation*, Kobe, Japan, May 12–17, 2009, 2009, pp. 3206–3211.
- [26] W. Birkfellner, *Applied Medical Image Processing*. Boca Raton: CRC Press, 2016.
- [27] M. A. Ulinuha, E. M. Yuniarno, S. M. S. Nugroho, and M. Hariadi, “Outer contour extraction of skull from CT scan images,” in *IOP Conference Series: Materials Science and Engineering. The International Conference on Information Technology and Digital Applications*, vol. 185, Yogyakarta, Indonesia, Nov. 14–16, 2016, 2016, Paper no. 012028.
- [28] M. A. Ulinuha, E. M. Yuniarno, M. Hariadi, and I. K. E. Purnama, “Extraction of skull and face surfaces from CT images,” in *International Conference of Artificial Intelligence and Information Technology*, Yogyakarta, Indonesia, Indonesia, Mar. 13–15, 2019, 2019, pp. 37–40.
- [29] K. Jordan and P. Mordohai, “A quantitative evaluation of surface normal estimation in point clouds,” in *International Conference on Intelligent Robots and Systems*, Chicago, IL, USA, Sep. 14–18, 2014, 2014, pp. 4220–4226.
- [30] T. Fawcett, “An introduction to ROC analysis,” *Pattern Recognit. Lett.*, vol. 27, no. 8, pp. 861–874, 2006.
- [31] J. Pont-Tuset and F. Marques, “Supervised evaluation of image segmentation and object proposal techniques,” *IEEE Trans. Pattern Anal. Mach. Intell.*, vol. 38, no. 7, pp. 1465–1478, 2016.